Chinese Journal of Chemical Engineering 46 (2022) 142–149

Contents lists available at ScienceDirect

Chinese Journal of Chemical Engineering

journal homepage: www.elsevier.com/locate/CJChE

Full Length Article

Hydrothermal preparation of Nb-doped $NaTaO_3$ with enhanced photocatalytic activity for removal of organic dye

Hao Zhou *, Qi Yin

State Key Laboratory of Clean Energy Utilization, Zhejiang University, Hangzhou 310027, China

ARTICLE INFO

Article history:
Received 4 January 2021
Received in revised form 30 April 2021
Accepted 21 May 2021
Available online 13 August 2021

Keywords:
Photocatalytic degradation
Methylene blue
$NaTaO_3$

ABSTRACT

The construction of efficient photocatalysts has received much attention in wastewater treatment. In this study, Nb-doped $NaTaO_3$ was prepared with different doping ratio by a facile hydrothermal method. The prepared catalysts were analyzed by X-ray diffraction, scanning electron microscopy, Brunauer-Emmett-Teller (BET) theory, ultraviolet–visible diffuse reflectance spectroscopy. Then the synthesized catalysts were employed to degrade a model pollutant, methylene blue (MB), under a 250 W mercury lamp. The characterization tests confirm that Nb was successfully doped into the crystal structure of $NaTaO_3$ and the modified $NaNb_xTa_{1-x}O_3$ (x is the doping ratio; x = 0.25, 0.5, 0.75) samples were formed, which were in regular cubic shapes just like pure $NaTaO_3$. The synthesized $NaNb_xTa_{1-x}O_3$ (x = 0.25, 0.5, 0.75) had improved specific surface area and narrowed band gaps compared with pure $NaTaO_3$. In photocatalytic degradation experiments, $NaNb_{0.75}Ta_{0.25}O_3$ presented the best photocatalytic activity ascribed to the narrow band gap and the high surface area, degradating 95.7% of MB after 180 min of reaction, which was even twice the ability of pure $NaTaO_3$. Besides, the effects of possible inorganic anions and cations in wastewater on photocatalytic degradation were investigated. Electron spin resonance (ESR) tests and capture experiments were also conducted and a possible photocatalytic mechanism was proposed. This work provides a direction for constructing superior $NaTaO_3$-based photocatalysts to be widely utilized in environmental protection.

1. Introduction

Large amounts of industrial wastewater and living sewage have been poured into water with accelerated industrialization and urbanization, resulting in serious damge to water resources. Dyes are one of the organic pollutants in water that cannot be ignored. Photocatalytic degradation technology has been developed under this background, which means decompose pollutants by adding photocatalyst to the pollutant system in the sunlight. This technology can completely oxidize various organic and inorganic pollutants with low operating cost and high degradation efficiency in comparison to other methods, which gives it broad prospect for application. Therefore, it is a long-term research project for worldwide scholars to find stable and efficient catalysts for photocatalytic degradation of pollutants like dyes in wastewater.

In recent years, a new kind of semiconductor material named perovskite has drawn great attention. Perovskite is a compound with the general molecular formula ABX_3 in which A and B refer to cations and X to anions. It was first discovered as calcium titanate ($CaTiO_3$) in perovskite, and was named after Russian geologist Lev Perovski in 1839 [1]. Later, perovskite-formed composite oxides have been considered as promising photocatalysts since Voorhoeve *et al.* [2] firstly discovered their high photocatalytic activity in the 1970s. Among various perovskites, $NaTaO_3$ is expected to be a promising photocatalyst due to its good structure and high charge separation efficiency. However, the high band-gap energy of $NaTaO_3$ hinders efficient utilization of solar light. Therefore, scholars across the world have done large amounts of modification on $NaTaO_3$ to further improve its photocatalytic activity, such as ion doping [3–7], heterojunctions [7–12], noble metal loading [12–15] and different crystal facets exposing [16]. It is worth mentioning that Wang *et al.* [5] prepared $NaNb_xTa_{1-x}O_3$ perovskite photocatalyst and applied it to photocatalytic degradation of pollutants for the first time. However, the molten salt method they used to prepare photocatalyst required a high reaction temperature, and the photocatalyst still had room for improvement in the light response.

Herein, we firstly reported a facile hydrothermal method to dope Nb into the crystal structrue of $NaTaO_3$. The synthesized

* Corresponding author.
E-mail address: zhouhao@zju.edu.cn (H. Zhou).

https://doi.org/10.1016/j.cjche.2021.05.037
1004-9541/

$NaNb_xTa_{1-x}O_3$ (x = 0.25, 0.5, 0.75), especially $NaNb_{0.75}Ta_{0.25}O_3$, exhibited superior photocatalytic activities compared with pure $NaTaO_3$ for degradation of a model pollutant, methylene blue (MB), in ultraviolet light. This should be attributed to improved specific surface area and narrowed band gaps, which is verified by a series of characterization tests. Besides, we investigated the effects of inorganic anions and cations that may exist in wastewater on photocatalytic degradation and proposed a possible photocatalytic mechanism over the catalysts we prepared.

2. Experimental

2.1. Chemicals

Sodium hydroxide (NaOH, AR), sodium chloride (NaCl, AR), sodium sulfate (Na_2SO_4, AR), sodium nitrate ($NaNO_3$, AR), calcium nitrate tetrahydrate ($Ca(NO_3)_2{\cdot}4H_2O$, 98.5%) were purchased from Sinopharm Chemical Regent Co. Ltd (Shanghai, China). Niobium oxide (Nb_2O_5, 99.9%), methylene blue (MB, biotechnology level), ferric sulfate nonahydrate ($Fe(NO_3)_3{\cdot}9H_2O$, 98.5%) were purchased from Shanghai Macklin Biochemical Co., Ltd. Tantalum oxide (Ta_2O_5, 99.99%) was purchased from Shanghai Adamas Reagent Co. LTD. *L*-ascorbic acid (99%) was purchased from Acros Organics USA Company. Isopropanol (IPA, 99.8%) was purchased from Aladdin Reagent (Shanghai) Co., LTD. Ethylenediaminetetraacetic acid disodium salt (EDTA-2Na, AR) was purchased from Beijing Bioss Biotechnology Co. LTD. All of the reagents were used without further purification.

2.2. Preparation

$NaNb_xTa_{1-x}O_3$ (x = 0, 0.25, 0.5, 0.75) photocatalysts were synthesized by a hydrothermal method based on the previous study [17]. In a typical procedure, 0.442 g Ta_2O_5 and 40 ml 1.5 $mol{\cdot}L^{-1}$ NaOH solution were added into a 50 ml Teflon-lined stainless-steel autoclave. The autoclave was sealed and kept at 140 °C for 12 h and then cooled to room temperature in air. The product was first washed with deionized water for several times, and then dried overnight at 80 °C to obtain $NaNb_xTa_{1-x}O_3$ (x = 0), namely pure $NaTaO_3$. For Nb-doped samples, the mass of Ta_2O_5 in the raw material was reduced while the mass of Nb_2O_5 was increased according to the molar ratio with remaining processes unchanged. The obtained catalysts were referred to as $NaNb_xTa_{1-x}O_3$ (x = 0.25, 0.5, 0.75), respectively.

2.3. Characterization

The crystal structures of prepared samples were characterized by X-ray diffraction (XRD) (Cu $K_{\alpha1}$ radiation, λ = 0.154 nm) for a test range of 2θ = 15°–90°. The microscopic morphologies were observed by scanning electron microscopy (SEM, Hitachi Su-8010), with an acceleration voltage of 5.0 kV. The Brunauer-Emmett-Teller (BET) theory was employed to determine the specific surface areas of the samples using nitrogen as the analysis gas. The degassing temperature was set at 423 K and the degassing time was 20 h. The ultraviolet-visible (UV-vis) diffuse reflectance spectra (DRS) were obtained by a UV-visible spectrophotometer (Shimazu UV-3600) with a scanning range of 200–600 nm.

2.4. Photocatalytic degradation experiment

The photocatalytic activities of prepared samples were evaluated by the degradation of MB using a 250 W mercury lamp. First, 50 mg catalyst was dispersed in 50 ml MB solution (10 $mg{\cdot}L^{-1}$). The suspension was stirred in the dark for 30 min to attain the adsorption–desorption equilibrium. Then it was exposed to the UV light and the reaction started. Stirring and water cooling were maintained throughout the reaction. Liquid samples were taken and separated with a syringe filter every 30 min. And a visible spectrophotometer (INESA 7230G) was employed to analyze their absorbance at 664 nm.

The absorbance A of the solution is proportional to the dye concentration C according to the Beer-Lambert law, so degradation efficiency η of the dye can be expressed as

$$\eta = \frac{C_0 - C}{C_0} = \frac{A_0 - A}{A_0} \tag{1}$$

C_0 and A_0 are the initial concentration and absorbance of the solution. C and A are the concentration and absorbance after irradiation for t time.

The kinetic process of photocatalytic reaction can be characterized by the Langmuir-Hinshelwood kinetic equation with the rate of degradation of reactants R expressed as

$$R = \frac{-\mathrm{d}C}{\mathrm{d}t} = \frac{k_1 k_2 C}{1 + k_2 C_0} \tag{2}$$

k_1 is the limiting rate constant of photocatalytic reaction; k_2 is the equilibrium constant of adsorption which is usually far less than 1.

After calculating the integration of the above formula, it can be expressed as

$$\ln\frac{C_0}{C} = k_{\mathrm{app}} t \tag{3}$$

This is the pseudo-first order correlation where k_{app} is the apparent rate constant of the photocatalytic reaction.

The slope can be obtained by linear fitting of experimental results according to the above formula. The value of the slope is the apparent rate constant k_{app}, which can characterize the activity of the catalyst quantitatively.

In order to explore the influence of anions (Cl^-, SO_4^{2-}, NO_3^-) in wastewater on photocatalytic activity, the corresponding sodium salts (0.1 $mol{\cdot}L^{-1}$) were added into MB solution, respectively. And the corresponding nitrates (0.1 $mol{\cdot}L^{-1}$) were employed to explore the influence of cations (Na^+, Ca^{2+}, Fe^{3+}).

Electron spin resonance (ESR) spectroscopic experiments were conducted on a Bruker EMXPLUS spectrometer to investigate the generated active free radicals over the catalyst under irradiation. The spin-trap reagents were 2,2,6,6-tetramethyl-1-piperidinyloxy (TEMPO) or 5,5-dimethyl-1-pyrroline *N*-oxide (DMPO) in water or methanol. Capture experiments were carried out in combination with ESR test results to identify the active free radicals involved in the reaction process. *L*-ascorbic acid, IPA and EDTA-2Na (1 $mmol{\cdot}L^{-1}$) were added to MB solution as scavengers of superoxide radicals ($\cdot O_2^-$), hydroxyl radicals ($\cdot$OH) and holes (h^+), respectively.

3. Results and Discussion

3.1. Characterization of as-prepared catalysts

The crystal structures of synthesized $NaNb_xTa_{1-x}O_3$ (x = 0, 0.25, 0.5, 0.75) were characterized by XRD, as shown in Fig. 1. When x = 0, the diffraction peaks at 22.8°, 32.4°, 46.6° and 52.5° were clearly observed, corresponding to (0 2 0), (1 2 1), (2 0 2), (2 2 2) planes of $NaTaO_3$ crystal, respectively. This was consistent with the standard card of orthorhombic $NaTaO_3$ crystal (PDF#73-0878, a = 5.521, b = 7.795, c = 5.484, $\alpha = \beta = \gamma$ = 90°) [5]. To our knowledge, the characteristic diffraction peaks of cubic $NaNbO_3$ crystal (PDF#75-2102, $a = b = c$ = 3.906, $\alpha = \beta = \gamma$ = 90°) are located at 22.7°, 32.4°, 46.5° and 52.3°, indexed to (1 0 0), (1 1 0), (2 0 0),

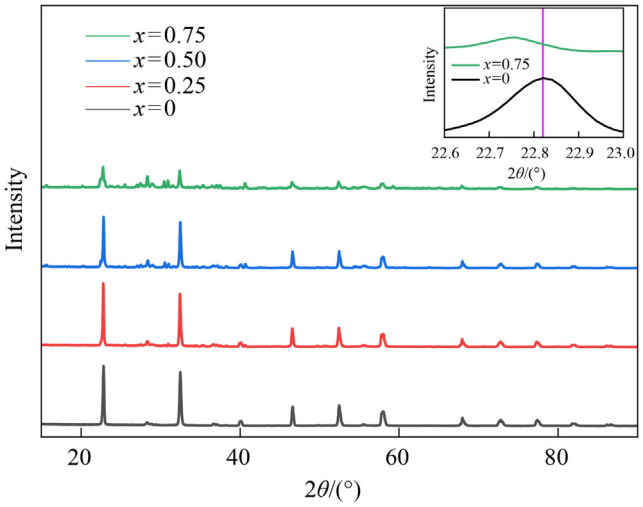

Fig. 1. XRD pattern of as-prepared $NaNb_xTa_{1-x}O_3$ (x = 0, 0.25, 0.5, 0.75).

(2 1 0) planes of $NaNbO_3$ crystal, respectively [18]. As shown in the enlarged part of the XRD pattern, the diffraction peak of Nb-doped $NaTaO_3$ was disorted at 22.8° and approached the characteristic diffraction peak of $NaNbO_3$ at 22.7°. Similar changes also occurred at other characteristic diffraction peaks. It can be inferred that Nb was successfully doped into the crystal structure of $NaTaO_3$ forming the modified $NaNb_xTa_{1-x}O_3$ crystal by adding a certain amount of Nb_2O_5 in the hydrothermal process.

The microscopic morphologies of the synthesized samples were observed by SEM (Fig. 2). It turns out that all samples were well-crystallized. Fig. 2(a) shows that the pure $NaTaO_3$ sample had regular cubic morphology with a particle size of about 1 μm. As shown in Fig. 2(b)–(d), the doped samples ($NaNb_xTa_{1-x}O_3$, x = 0.25, 0.5, 0.75) also had regular cubic morphologies similar to pure $NaTaO_3$ sample. However, the particle size of the doped samples was reduced to a certain extent, falling in the range of less than 1. The results of BET tests (Table 1) agree well with the phenomena observed by SEM. The specific surface area of $NaNb_xTa_{1-x}O_3$ was 0.8063, 0.9813, 1.737, 2.502 $m^2 \cdot g^{-1}$ corresponding to x = 0, 0.25, 0.5, 0.75, respectively. It is obvious that the specific surface area increased gradually with the increase of Nb-doping ratio. $NaNb_{0.75}Ta_{0.25}O_3$ had the largest specific surface area, which was more than three times of pure $NaTaO_3$. As is known that the specific surface area of catalysts has a significant influence on their catalytic activities. The Nb-doped samples were expected to perform well in the photocatalytic reaction from the results of SEM and BET tests.

The optical properties of synthesized $NaNb_xTa_{1-x}O_3$ (x = 0, 0.25, 0.5, 0.75) were characterized through a DRS pattern as shown in Fig. 3. It is obvious that pure $NaTaO_3$ only had strong absorption in the ultraviolet region with an absorption threshold (λ_g) of around 325 nm. Compared with the pure $NaTaO_3$ sample, the absorption regions of Nb-doped samples ($NaNb_xTa_{1-x}O_3$, x = 0.25, 0.5, 0.75) presented a significant phenomenon of redshift, with the absorption thresholds extending to about 366, 382, 416 nm, respectively. It cannot be neglected that the redshift became more obvious with the increase of Nb-doping ratio, and $NaNb_{0.75}Ta_{0.25}O_3$ had the largest absorption region. This may be attributed to the substitution of Ta^{5+} by Nb^{5+} in the $NaTaO_3$ photocatalysts [5]. The values of band gap energy (E_g, eV) for $NaNb_xTa_{1-x}O_3$ (x = 0, 0.25, 0.5, 0.75) were calculated as 3.82, 3.39, 3.25, 2.98 eV, respectively, according to the equation [4,9]

$$E_g = \frac{1240}{\lambda_g} \tag{4}$$

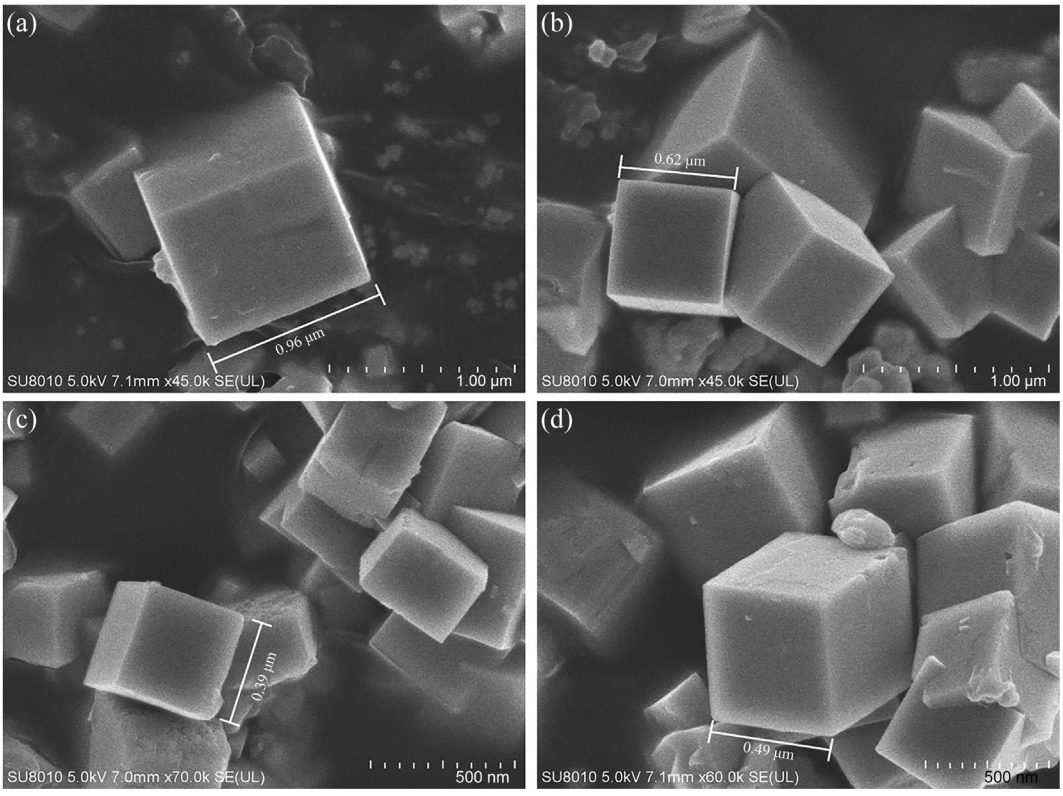

Fig. 2. SEM images of $NaNb_xTa_{1-x}O_3$ (a) x = 0, (b) x = 0.25, (c) x = 0.5, (d) x = 0.75.

Table 1
Specific surface area of $NaNb_xTa_{1-x}O_3$ (x = 0, 0.25, 0.5, 0.75)

x	Specific surface area/$m^2 \cdot g^{-1}$
0	0.8063
0.25	0.9813
0.5	1.737
0.75	2.502

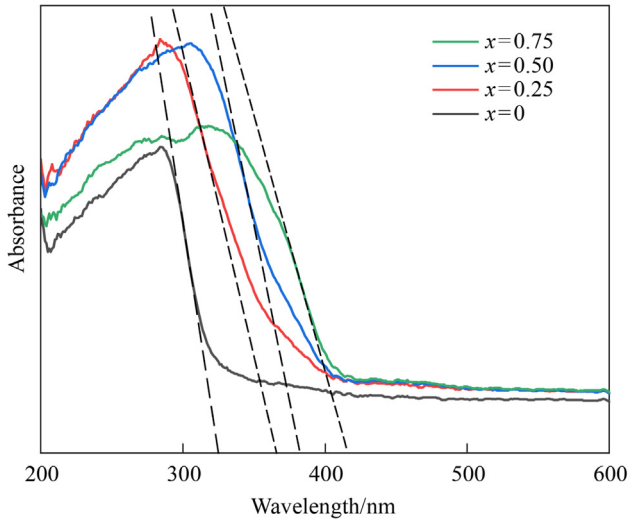

Fig. 3. UV–vis diffuse reflectance spectra of $NaNb_xTa_{1-x}O_3$ (x = 0, 0.25, 0.5, 0.75).

The decrease in the band gap energy can be explained by the locations of the valence and conduction bands of the prepared catalysts. The valence band potential of $NaNb_xTa_{1-x}O_3$ (x = 0, 0.25, 0.5, 0.75) was meant to be similar, due to the valence bands all consisting of O_{2p} orbitals. However, the conduction band potential of $NaNb_xTa_{1-x}O_3$ growed less negative with more accumulation of Nb_{4d} states, because the potential energy of Ta_{5d} orbital is higher than the Nb_{4d} orbital. Therefore, the band gap energy of $NaNb_xTa_{1-x}O_3$ (x = 0, 0.25, 0.5, 0.75) decreased in the following order: $NaTaO_3$ > $NaNb_{0.25}Ta_{0.75}O_3$ > $NaNb_{0.5}Ta_{0.5}O_3$ > $NaNb_{0.75}Ta_{0.25}O_3$ [19]. In addition to the redshift, the absorption intensity of doped samples in the ultraviolet region was also enhanced to different degrees as shown in the pattern. The absorption enhancement of $NaNb_{0.25}Ta_{0.75}O_3$ and $NaNb_{0.5}Ta_{0.5}O_3$ was particularyly obvious. The Nb-doped samples were expected to perform better photocatalytic activities due to the enhanced light absorption in the entire ultraviolet and visible region.

3.2. Photocatalytic performance

3.2.1. Optimal ratio of Nb-doping

The photocatalytic degradation of MB on $NaNb_xTa_{1-x}O_3$ (x = 0, 0.25, 0.5, 0.75) under the 250 W mercury lamp is shown in Fig. 4(a). It can be seen that the concentrations of MB all decreased over different samples during – 30–0 min. It was due to the dye molecules adsorbed by the catalyst. The ability of different catalysts to adsorb dyes was in the following order from small to large: $NaTaO_3$ < $NaNb_{0.25}Ta_{0.75}O_3$ < $NaNb_{0.5}Ta_{0.5}O_3$ < $NaNb_{0.75}Ta_{0.25}O_3$, agreeing with the results of BET tests. This was because the adsorption phenomenon took place at the surface of the samples [20]. Possible adsorption mechanisms include functional groups, charge, and active sites of the samples [21]. A few literatures have focused on the adsorption behavior of dye molecules on adsorbents [20,22].

However, this paper is meant to focus on the photocatalytic activities of the prepared samples as photocatalysts in the process of photocatalytic degradation. It is obvious that the concentrations of MB continuously declined since the light was turned on at 0 min as what Fig. 4(a) shows. After 180 min of reaction, the concentration of MB decreased to 53.0% of the initial value using $NaTaO_3$ as the photocatalyst, meaning that the degradation proportion was 47.0%. With more Nb doped in the prepared samples, they performed better photocatalytic activities. The degradation efficiency of MB was 87.4% and 93.1% over $NaNb_{0.25}Ta_{0.75}O_3$ and $NaNb_{0.5}Ta_{0.5}O_3$, respectively. $NaNb_{0.75}Ta_{0.25}O_3$ was the best photocatalyst in this paper, degradating 95.7% of MB after 180 min of reaction, which was even twice the ability of pure $NaTaO_3$. This was in great agreement with the results of BET tests and the UV–vis diffuse reflectance spectra. According to the above discussion, the following factors account for the high photocatalytic activity of $NaNb_{0.75}Ta_{0.25}O_3$. First, its narrowed band gap can improve the utilization of ultraviolet and visble light. Second, the high surface area can facilitate transport of substrate to the active sites of catalyst, hence enhancing the photocatalytic efficiency. Fig. 4(b) shows the reaction kinetic curves of MB degradated over the prepared samples. It can be concluded from the figure that the degradation process follows the pseudo-first-order kinetics. The apparent rate constants were 0.00313, 0.00924, 0.01090, 0.01241 min^{-1}, for $NaTaO_3$, $NaNb_{0.25}Ta_{0.75}O_3$, $NaNb_{0.5}Ta_{0.5}O_3$, $NaNb_{0.75}Ta_{0.25}O_3$, respectively. The constants can intuitively reflect the photocatalytic activities of prepared samples fitting well with Fig. 4(a).

It should be noted that the concentration of MB maintained at a high level (79.8% of the initial concentration after 180 min of irradiation) without any catalyst added in the solution. This control experiment indicates that the degradation of MB as shown in Fig. 4 should be attributed to the catalysts we prepared.

3.2.2. Influence of inorganic salt ions in wastewater

Inorganic salts in wastewater may have impacts on the removal process of pollutants [12,23]. In order to explore the influence of anions (Cl^-, SO_4^{2-}, NO_3^-) in wastewater on $NaNb_{0.75}Ta_{0.25}O_3$, the corresponding sodium salts (0.1 $mol \cdot L^{-1}$) were added into MB solution, respectively (Fig. 5). It can be concluded easily from Fig. 5(a) that all the inorganic salt ions in the wastewater had an obvious inhibitory effect on the absorption process. This may be because that large amounts of ions were adsorbed on the surface of samples which affected the surface charge and the electrostatic interaction with dye molecule [24]. It is obvious in Fig. 5(a) that SO_4^{2-} and Cl^- inhibited the photocatalytic degradation of MB on the catalyst. However, the rate of photocatalytic degradation was slightly increased after the addition of NO_3^-. The dynamic analysis in Fig. 5(b) supports the above conclusions. The apparent rate constants were 0.00278, 0.00389, 0.01616 min^{-1} after the addition of SO_4^{2-}, Cl^-, NO_3^-, respectively, while the constant was 0.01241 min^{-1} for the blank experiment. These phenomena can be explained by Eqs. (5)–(11) [25,26]. Free radicals like h^+ and ·OH are active substances that takes effect in photocatalytic degradation, which was verified in Section 3.3. To our knowledge, SO_4^{2-} can act as a scavenger reacting with h^+ and ·OH and producing the sulfate radical, $\cdot SO_4^-$. Though $\cdot SO_4^-$ is a very strong oxidant (redox potential = +2.6 eV) [25], its oxidation capacity is inferior to the photo-generated h^+ over $NaNb_{0.75}Ta_{0.25}O_3$. The estimated valence band potential of pure $NaTaO_3$ prepared by hydrothermal method is +3.0 eV according to previous studies [10,12]. The valence band potential of $NaNb_{0.75}Ta_{0.25}O_3$ in this paper can be regarded as around +3.0 eV, which was more positive than the redox potential of $\cdot SO_4^-$, as the doping of Nb had no effect on the valence band potential as analyzed in Section 3.1. And this leads to the superior oxidation capacity of photo-generated h^+ over

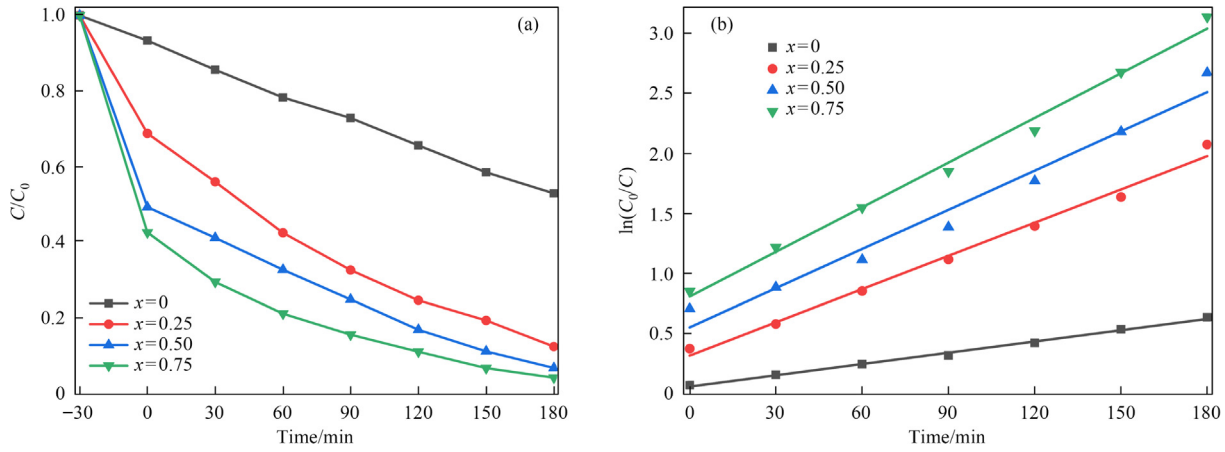

Fig. 4. (a) Photocatalytic degradation curves of MB over $NaNb_xTa_{1-x}O_3$ (x = 0, 0.25, 0.5, 0.75) under 250 W Hg lamp and (b) corresponding reaction kinetic curves.

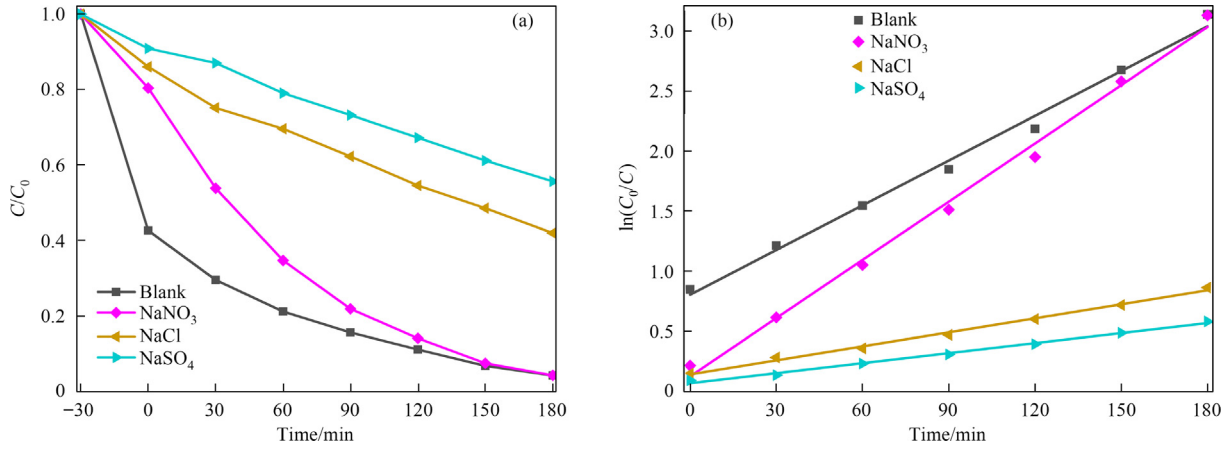

Fig. 5. (a) Effects of anions on the photocatalytic degradation of MB over $NaNb_{0.75}Ta_{0.25}O_3$ under 250 W Hg lamp and (b) corresponding reaction kinetic curves.

$NaNb_{0.75}Ta_{0.25}O_3$ compared with $\cdot SO_4^-$. Therefore, the decrease of degradation efficiency after the addition of SO_4^{2-} can be attributed to the photo-generated h^+ over $NaNb_{0.75}Ta_{0.25}O_3$ replaced by $\cdot SO_4^-$. The reason for Cl^- inhibiting the photocatalytic degradation is similar to that of SO_4^{2-} [26,27]. In contrast to SO_4^{2-} and Cl^-, NO_3^- can support the direct or indirect formation of ·OH in the presence of photons, resulting in the slight increase of the degradation rate.

$$SO_4^{2-} + h^+ \rightarrow \cdot SO_4^- \quad (5)$$

$$SO_4^{2-} + \cdot OH \rightarrow \cdot SO_4^- + OH^- \quad (6)$$

$$Cl^- + h^+ \rightarrow \cdot Cl \quad (7)$$

$$Cl^- + \cdot OH \rightarrow \cdot Cl + OH^- \quad (8)$$

$$NO_3^- + h\nu \rightarrow NO_2 + \cdot O^- \quad (9)$$

$$\cdot O^- + H_2O \rightarrow \cdot OH + OH^- \quad (10)$$

$$NO_3^- + h\nu + H_2O \rightarrow NO_2 + \cdot OH + OH^- \quad (11)$$

In order to explore the effects of cations (Na^+, Ca^{2+}, Fe^{3+}) in the wastewater on photocatalytic degradation, the corresponding nitrate (0.1 mol·L^{-1}) was added to the MB solution (Fig. 6). The results in Fig. 6(a) reflect that the reaction rate slightly increased with the addition of Na^+ or Ca^{2+}. The apparent rate constants were 0.01616, 0.01855 min^{-1} after the addition of Na^+, Ca^{2+}, respectively, while the constant was 0.01241 min^{-1} for the blank experiment as in Fig. 6(b). Considering the effect of nitrate ion, it can be concluded that Na^+ and Ca^{2+} have little influence on photocatalytic degradation process. However, the degradation efficiency reached almost 100% within 10 min after Fe^{3+} was added, which is not shown in Fig. 6. It is obvious that Fe^{3+} can remarkably enhance the degradation rate of MB, which can be explained in two ways. For one thing, Fe^{3+} can unite with photogenerated electrons and holes forming Fe^{2+} and Fe^{4+} ions, which promotes the separation of electrons and holes. For another, Fe^{3+}, as an effective photosensitive substance, can produce ·OH under weak acidic conditions after adsorbing light. This accelerates the degradation process resembling the photo-Fenton reactions [12].

3.3. Possible photocatalytic mechanism

ESR tests were conducted to directly investigate the generated reactive oxygen species and radicals over $NaNb_{0.75}Ta_{0.25}O_3$ under irradiation. Fig. 7(a)–(c) present the ESR spectra for the detection of h^+, ·OH, and $\cdot O_2^-$, respectively. Under the dark condition, the signal of the spin-trap reagent, TEMPO, was observed as in Fig. 7(a). The signal decreased when the UV light was on, which was due to the combination of TEMPO and h^+ to form $TEMPO^+$. This indicates that the electrons transit from the valence band to the conduction band after the catalyst absorbing photons, leaving active h^+ in the valence band. The characteristic signals of the

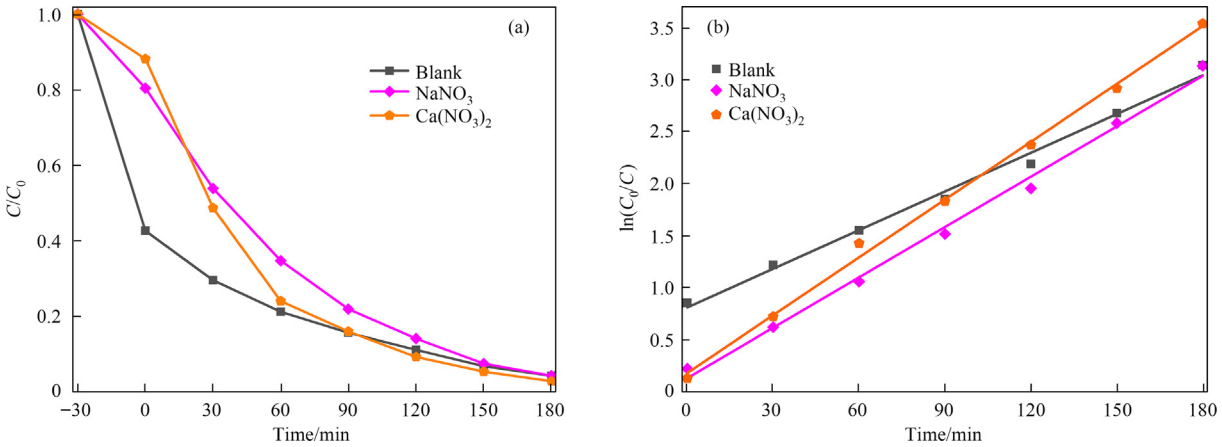

Fig. 6. (a) Effects of cations on the photocatalytic degradation of MB over $NaNb_{0.75}Ta_{0.25}O_3$ under 250 W Hg lamp and (b) corresponding reaction kinetic curves.

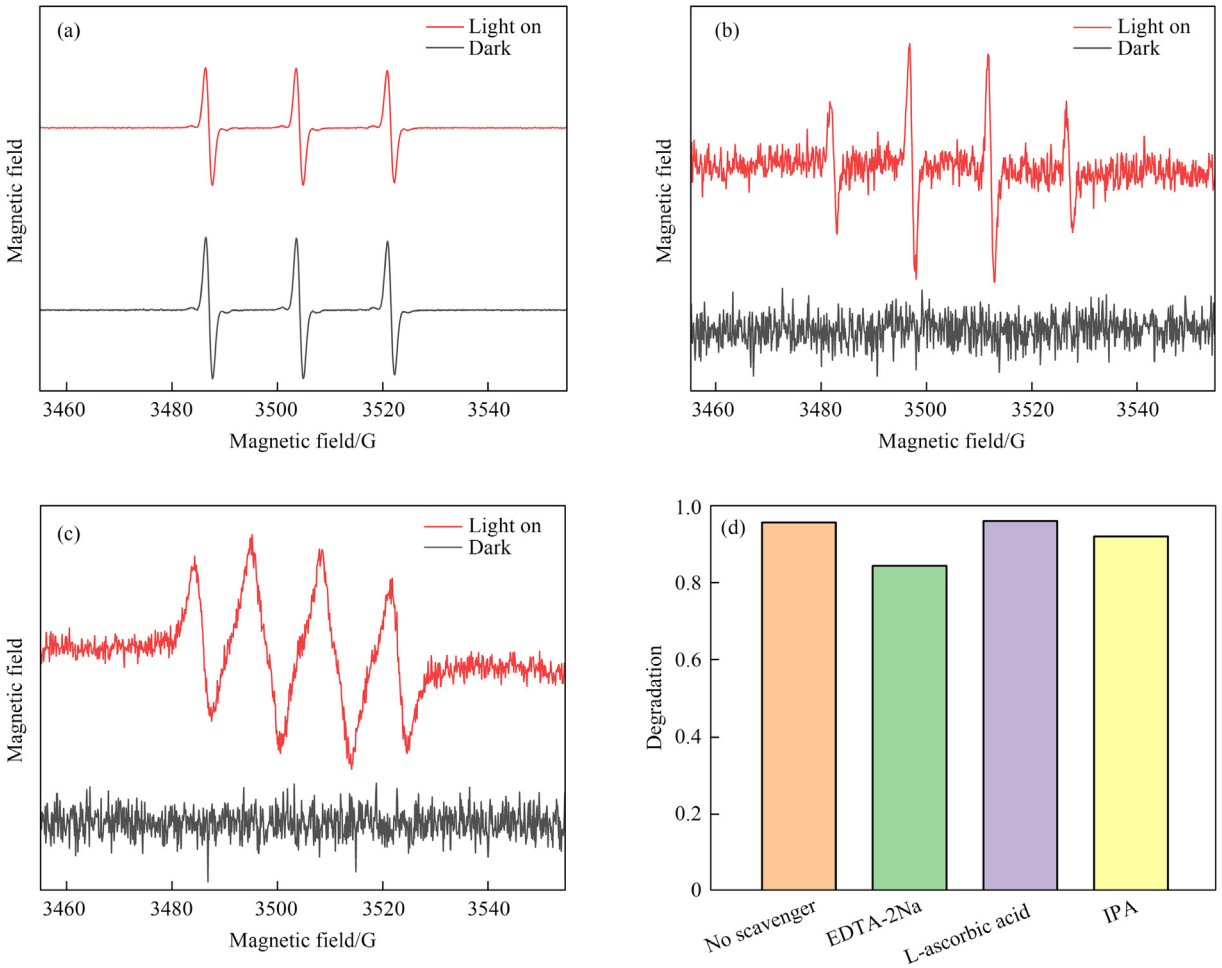

Fig. 7. ESR tests of (a) h^+, (b) ·OH, (c) $\cdot O_2^-$ and (d) Photocatalytic degradation efficiency of MB under 250 W Hg lamp in the absence or presence of scavengers (EDTA-2Na, L-ascorbic acid, IPA) over $NaNb_{0.75}Ta_{0.25}O_3$.

DMPO-·OH [27,28] appeared after the UV light was on as Fig. 7(b) shows, which confirms that ·OH was formed over the catalyst under irradiation. Fig. 7(c) shows that the characteristic signals of DMPO-$\cdot O_2^-$ [11,28] were detected under the UV light, indicating that $\cdot O_2^-$ was also generated.

However, the ESR tests can only qualitatively verify the active substances produced on the catalyst. It needs to be combined with the capture experiments to determine the dominant active free radicals in the reaction process, as Fig. 7(d) shows. *L*-ascorbic acid, IPA and EDTA-2Na (1 $mmol \cdot L^{-1}$) were added to MB solution as scavengers of $\cdot O_2^-$, ·OH, and h^+, respectively. The results reflect that the degradation efficiency decreased the most after adding EDTA-2Na, followed by IPA. This indicates that h^+ mainly plays a driving role in the degradation process. And ·OH also takes effect to a cer-

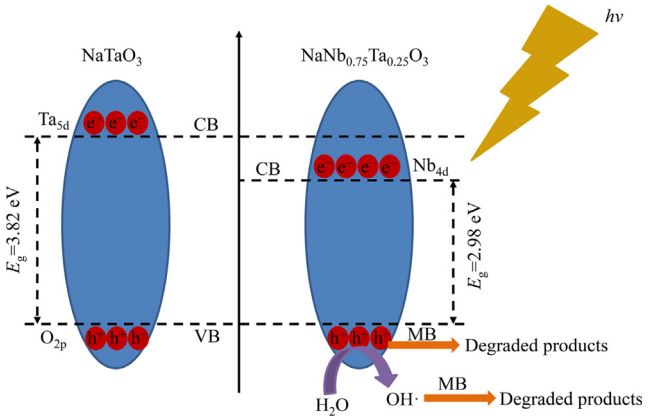

Fig. 8. Schematic model of a possible photocatalytic mechanism over $NaNb_{0.75}Ta_{0.25}O_3$.

tain extent during the reation process. The degradation efficiency did not decrease, but even increased slightly in the presence of L-ascorbic acid. This indicates that only a trace amount of $\cdot O_2^-$ was generated on the catalyst, which has little effect on the degradation process. The slight increase of degradation efficiency may be due to the capturing effect of L-ascorbic acid on $\cdot O_2^-$, which is positive for Eq. (12) [12]. This causes more electrons to be consumed, promoting the separation of electron-hole pairs and making more h^+ participate in the reaction. Hence, it can be summarized that h^+ and $\cdot OH$ are the main active substances in the photocatalytic degradation process of MB over $NaNb_{0.75}Ta_{0.25}O_3$.

$$O_2 + e^- \rightarrow \cdot O_2^- \quad (12)$$

Fig. 8 shows the proposed mechanism how Nb-doping improves the photocatalytic activity of $NaTaO_3$. Substitution of Ta within the $NaTaO_3$ lattice by Nb creates an additional energy level just below the Ta_{5d} orbital as the new hybrid Ta_{5d} and Nb_{4d} orbitals. This makes the conduction band potential of $NaNb_{0.75}Ta_{0.25}O_3$ less negative than pure $NaTaO_3$. Therefore, the band gap energy of $NaNb_{0.75}Ta_{0.25}O_3$ decreases to 2.98 eV from 3.82 eV of pure $NaTaO_3$, and this improves the utilization of light. When the light is incident on the surface of $NaNb_{0.75}Ta_{0.25}O_3$, the electrons in the valence band transit easily to the conduction band, leaving active h^+ in the valence band. The h^+ can not only directly oxidize MB, but also react with H_2O to generate $\cdot OH$, which can also degradate MB. Besides, the higher surface area of $NaNb_{0.75}Ta_{0.25}O_3$ facilitates the degradation of MB and the conversion of H_2O to $\cdot OH$ by h^+. Thus, the superior photocatalytic activity of $NaNb_{0.75}Ta_{0.25}O_3$ can be attributed to the narrow band gap and the high surface area.

4. Conclusions

In this study, Nb was successfully doped into the $NaTaO_3$ lattice to form $NaNb_xTa_{1-x}O_3$ (x = 0, 0.25, 0.5, 0.75) photocatalysts with regular cubic shapes through hydrothermal method. Among the synthesized samples in this paper, $NaNb_{0.75}Ta_{0.25}O_3$ exhibited the best photocatalyst acitivity, degradating 95.7% of MB after 180 minutes of irradiation under a 250 W mercury lamp, which was even twice the ability of pure $NaTaO_3$. The excellent photocatalytic activity of $NaNb_{0.75}Ta_{0.25}O_3$ is ascribed to the narrowed band gap (2.98 eV) and the increased surface area (2.502 $m^2 \cdot g^{-1}$) compared with pure $NaTaO_3$ (3.82 eV, 0.8063 $m^2 \cdot g^{-1}$) according to the results of various characterization tests. Influences of various anions and cations in wastewater on the photocatalytic activity of $NaNb_{0.75}Ta_{0.25}O_3$ were explored. SO_4^{2-} and Cl^- inhibited the photocatalytic degradation of MB on $NaNb_{0.75}Ta_{0.25}O_3$ due to the scavenging effect on h^+ and $\cdot OH$, while NO_3^- increased the rate of photocatalytic degradation slightly because of the promotion for the direct or indirect formation of $\cdot OH$ under irradiation. Fe^{3+} remarkably enhanced the degradation rate of MB, because it can promote the separation of electrons and holes and produce $\cdot OH$ under weak acidic conditions after adsorbing light. This study provides a direction for constructing novel efficient photocatalysts, making it possible for superior $NaTaO_3$-based photocatalysts to be widely utilized in environmental protection.

Declaration of Competing Interest

The authors declare that they have no known competing financial interests or personal relationships that could have appeared to influence the work reported in this paper.

Acknowledgements

This work was supported by the Innovative Research Groups of the National Natural Science Foundation of China (51621005).

References

[1] M.A. Green, A. Ho-Baillie, H.J. Snaith, The emergence of perovskite solar cells, *Nat. Photonics* 8 (7) (2014) 506–514.
[2] R.J. Voorhoeve, D.W. Johnson, J.P. Remeika, P.K. Gallagher, Perovskite oxides: Materials science in catalysis, *Science* 195 (4281) (1977) 827–833.
[3] S. Wang, X. Xu, H. Luo, Y. Bai, S. Abbas, J. Zhang, J. Zhao, C. Tang, Enhanced organic dye removal of the W and N co-doped $NaTaO_3$ under visible light irradiation, *J. Alloy. Compd.* 681 (2016) 225–232.
[4] H. Li, X.B. Shi, X.G. Liu, X. Li, Synthesis of novel, visible-light driven S, N-doped $NaTaO_3$ catalysts with high photocatalytic activity, *Appl. Surf. Sci.* 508 (2020) 145306.
[5] M. Wang, M. Fang, X. Min, Z. Huang, C. Tang, Y. Liu, X. Wu, Molten salt synthesis of $NaNb_xTa_{1-x}O_3$ perovskites with enhanced photocatalytic activity, *Chem. Phys. Lett.* 686 (2017) 18–25.
[6] C.C. Hu, H.H. Huang, Y.C. Huang, N-doped $NaTaO_3$ synthesized from a hydrothermal method for photocatalytic water splitting under visible light irradiation, *J. Energy Chem.* 26 (3) (2017) 515–521.
[7] S. Wang, X.W. Xu, H. Luo, C.C. Cao, X.Y. Song, J.L. Zhao, J. Zhang, C.C. Tang, Novel $SrTiO_3/NaTaO_3$ and visible-light-driven $SrTiO_3/NaTaO_3$: N nano-heterojunctions with high interface-lattice matching for efficient photocatalytic removal of organic dye, *RSC Adv.* 8 (34) (2018) 19279–19288.
[8] S. Yang, D. Xu, B. Chen, B. Luo, X.u. Yan, L. Xiao, W. Shi, Synthesis and visible-light-driven photocatalytic activity of p-n heterojunction $Ag_2O/NaTaO_3$ nanocubes, *Appl. Surf. Sci.* 383 (2016) 214–221.
[9] X. Wang, J. Ma, Y. Kong, C. Fan, M. Peng, S. Komarneni, Synthesis of p-n heterojunction $Ag_3PO_4/NaTaO_3$ composite photocatalyst for enhanced visible-light-driven photocatalytic performance, *Mater. Lett.* 251 (2019) 192–195.
[10] A.P. Singh, S. Kumar, M. Thirumal, Efficient charge transfer in heterostructures of $CdS/NaTaO_3$ with improved visible-light-driven photocatalytic activity, *ACS Omega* 4 (7) (2019) 12175–12185.
[11] E.T. Cui, G.H. Hou, X.H. Chen, F. Zhang, Y.X. Deng, G.Y. Yu, B.B. Li, Y.Q. Wu, *In-situ* hydrothermal fabrication of $Sr_2FeTaO_6/NaTaO_3$ heterojunction photocatalyst aimed at the effective promotion of electron-hole separation and visible-light absorption, *Appl. Catal. B: Environ.* 241 (2019) 52–65.
[12] L. Tang, C.Y. Feng, Y.C. Deng, G.M. Zeng, J.J. Wang, Y.N. Liu, H.P. Feng, J.J. Wang, Enhanced photocatalytic activity of ternary $Ag/g\text{-}C_3N_4/NaTaO_3$ photocatalysts under wide spectrum light radiation: The high potential band protection mechanism, *Appl. Catal. B: Environ.* 230 (2018) 102–114.
[13] D.B. Xu, W.D. Shi, C.J. Song, M. Chen, S.B. Yang, W.Q. Fan, B.Y. Chen, *In-situ* synthesis and enhanced photocatalytic activity of visible-light-driven plasmonic $Ag/AgCl/NaTaO_3$ nanocubes photocatalysts, *Appl. Catal. B: Environ.* 191 (2016) 228–234.
[14] V. Jeyalakshmi, R. Mahalakshmy, K.R. Krishnamurthy, B. Viswanathan, Photocatalytic reduction of carbon dioxide in alkaline medium on La modified sodium tantalate with different co-catalysts under UV-visible radiation, *Catal. Today* 266 (2016) 160–167.
[15] M. Li, P. Li, K. Chang, T. Wang, L.Q. Liu, Q. Kang, S.X. Ouyang, J.H. Ye, Highly efficient and stable photocatalytic reduction of CO_2 to CH_4 over Ru loaded $NaTaO_3$, *Chem. Commun. (Camb.)* 51 (36) (2015) 7645–7648.
[16] Q. Zhang, Z. Li, S. Wang, R. Li, X. Zhang, Z. Liang, H. Han, S. Liao, C. Li, Effect of redox cocatalysts location on photocatalytic overall water splitting over cubic $NaTaO_3$ semiconductor crystals exposed with equivalent facets, *ACS Catal.* 6 (4) (2016) 2182–2191.
[17] T. Xiang, F. Xin, J.S. Chen, Y.W. Wang, X.H. Yin, X. Shao, Selective photocatalytic reduction of CO_2 to methanol in CuO-loaded $NaTaO_3$ nanocubes in isopropanol, *Beilstein J. Nanotechnol.* 7 (2016) 776–783.

[18] W. Chen, Y. Hu, M. Ba, Surface interaction between cubic phase $NaNbO_3$ nanoflowers and Ru nanoparticles for enhancing visible-light driven photosensitized photocatalysis, *Appl. Surf. Sci.* 435 (2018) 483–493.
[19] P. Jana, V.A. de la Peña O'Shea, C.M. Montero, P. Gálvez, P. Pizarro, J.M. Coronado, D.P. Serrano, Mixed $NaNb_xTa_{1-x}O_3$ perovskites as photocatalysts for H_2 production, *Green Chem.* 17 (3) (2015) 1735–1743.
[20] U. Pal, A. Sandoval, S.I.U. Madrid, G. Corro, V. Sharma, P. Mohanty, Mixed titanium, silicon, and aluminum oxide nanostructures as novel adsorbent for removal of rhodamine 6G and methylene blue as cationic dyes from aqueous solution, *Chemosphere* 163 (2016) 142–152.
[21] N. Yahya, F. Aziz, N.A. Jamaludin, M.A. Mutalib, A.F. Ismail, W.N.W. Salleh, J. Jaafar, N. Yusof, N.A. Ludin, A review of integrated photocatalyst adsorbents for wastewater treatment, *J. Environ. Chem. Eng.* 6 (6) (2018) 7411–7425.
[22] S.A. Hassanzadeh-Tabrizi, M.M. Motlagh, S. Salahshour, Synthesis of ZnO/CuO nanocomposite immobilized on γ-Al_2O_3 and application for removal of methyl orange, *Appl. Surf. Sci.* 384 (2016) 237–243.
[23] B. Zhang, D. Zhang, Z. Xi, P. Wang, X. Pu, X. Shao, S. Yao, Synthesis of Ag_2O/$NaNbO_3$ p-n junction photocatalysts with improved visible light photocatalytic activities, *Sep. Purif. Technol.* 178 (2017) 130–137.
[24] Y.M. Yue, P.X. Zhang, W. Wang, Y.C. Cai, F.T. Tan, X.Y. Wang, X.L. Qiao, P.K. Wong, Enhanced dark adsorption and visible-light-driven photocatalytic properties of narrower-band-gap Cu_2S decorated Cu_2O nanocomposites for efficient removal of organic pollutants, *J. Hazard. Mater.* 384 (2020) 121302.
[25] Y.P. Ong, L.N. Ho, S.A. Ong, J. Banjuraizah, A.H. Ibrahim, S.L. Lee, N. Nordin, Comparative study of different polyatomic ions of electrolytes on electricity generation and dye decolourization in photocatalytic fuel cell, *J. Water Process. Eng.* 37 (2020) 101479.
[26] R. Saleh, A. Taufik, S.P. Prakoso, Fabrication of Ag_2O/TiO_2 composites on nanographene platelets for the removal of organic pollutants: Influence of oxidants and inorganic anions, *Appl. Surf. Sci.* 480 (2019) 697–708.
[27] J. Li, K.M. Zhu, R.M. Li, X.H. Fan, H. Lin, H. Zhang, The removal of azo dye from aqueous solution by oxidation with peroxydisulfate in the presence of granular activated carbon: Performance, mechanism and reusability, *Chemosphere* 259 (2020) 127400.
[28] L. Cao, C. Yang, B. Zhang, K. Lv, M. Li, K. Deng, Synergistic photocatalytic performance of cobalt tetra(2-hydroxymethyl-1, 4-dithiin)porphyrazine loaded on zinc oxide nanoparticles, *J. Hazard. Mater.* 359 (2018) 388–395.